Electrochimica Acta 197 (2016) 84–91

Contents lists available at ScienceDirect

Electrochimica Acta

journal homepage: www.elsevier.com/locate/electacta

Interactions between Graphene and Ionic Liquid Electrolyte in Supercapacitors

Jing Li[a,b], Jie Tang[a,b,*], Jinshi Yuan[a], Kun Zhang[a], Qingguo Shao[a], Yige Sun[a,b], Lu-Chang Qin[c,d,*]

[a] National Institute for Materials Science, 1-2-1 Sengen, Tsukuba, Ibaraki 305-0047, Japan
[b] Doctoral Program in Materials Science and Engineering, University of Tsukuba, 1-1-1 Tennodai, Tsukuba, Ibaraki 305-0006, Japan
[c] Ningbo Institute of Materials Technology and Engineering, Chinese Academy of Sciences, Ningbo 315201, China
[d] Department of Physics and Astronomy, University of North Carolina at Chapel Hill, Chapel Hill, NC 27599-3255, USA

ARTICLE INFO

Article history:
Received 14 December 2015
Received in revised form 27 February 2016
Accepted 6 March 2016
Available online 8 March 2016

Keywords:
Graphene
Supercapacitor
Ionic liquid

ABSTRACT

The graphene material prepared by the chemical reduction method usually has oxygenic functional groups in it and such functional groups often result in interactions between the graphene electrode and the electrolyte in supercapacitors. We have examined the existential form of interactions between graphene as the electrode and three kinds of ionic liquid, 1-ethyl-3-methylimidazolium bis (trifluoromethylsulfonyl) imide (EMI-TFSI), 1-ethyl-3-methylimidazolium tetrafluoroborate (EMI-BF_4), and 1-methyl-1-propylpiperidinium bis (trifluoromethyl sulfonyl) imide (MPPp-TFSI), as the electrolyte of a supercapacitor. Mass spectroscopy (MS) and Fourier transform infrared spectroscopy (FT-IR) analyses confirmed that the residual hydroxyl groups in graphene were transferred to EMI^+ and $TFSI^-$ lost oxygen atoms to graphene, while little reaction took place in BF_4^- or $MPPp^+$, during the process of charging. The chemical reactions are suggested to contribute to the device capacitance while it is also one of the reasons for the decreased electrochemical stability window. In this study the highest energy density achieved using the graphene electrode is 169 Wh kg^{-1} in MPPp-TFSI electrolyte charged to 4.4 V.

1. Introduction

To meet the growing energy demand, many devices have been developed for energy storage applications. To evaluate the performance of an energy storage device, two quantities are commonly used: the energy density and power density. Higher energy density will lead to a longer service time and higher power density means a shorter charging/discharging time. Compared with other energy storage devices, the merits of electric double-layer capacitors, which are also often called supercapacitors, are their high power density and long lifetime [1]. To improve its energy density while keeping its high power density, various structures of carbon have been the material of choice for the electrode [2–4]. In recent years, graphene has attracted a lot of attention for the application as supercapacitor electrode material due to its excellent conductivity and large specific surface area owing to its unique two-dimensional structure [5–9].

However, there are still problems that have limited the further improvement of energy density in supercapacitors with graphene electrodes. One is the re-stacking of graphene sheets due to the van der Waals attractions after reduction, which will decrease the specific surface area [10]. To solve this problem, single-wall carbon nanotubes (SWNTs) and graphene (SWNT/graphene) composites have been developed which exhibited great advantages as the active material for supercapacitor electrodes [7,11].

Besides the electrode materials, the electrolyte will also have a significant impact on the performance of supercapacitors. Various ionic liquids have been investigated as the electrolyte to take advantage of their wider electrochemical stability window [12–14]. The interactions between the carbon electrode and the ionic liquid electrolyte also affect the electrochemical performance of the supercapacitors. In particular, the oxygenic functional groups on the carbon electrode can involve substantial interfacial interactions with the ionic liquid electrolyte as having been demonstrated both experimentally and theoretically [14–19]. In this study, using mass spectroscopy (MS), Fourier transform infrared spectroscopy (FT-IR), and electrochemical characterization techniques, we have examined three different ionic liquids to investigate their respective electrochemical reactions with the

* Corresponding author. Tel.: +81 29 859 2728; fax: +81 29 859 2701.
E-mail addresses: tang.jie@nims.go.jp, lcqin@unc.edu (J. Tang).

http://dx.doi.org/10.1016/j.electacta.2016.03.036
0013-4686/

SWNT/graphene electrode when the ionic liquid was used as the electrolyte in a symmetric supercapacitor: 1-ethyl-3-methylimidazolium bis (trifluoromethylsulfonyl) imide (EMI-TFSI), 1-ethyl-3-methylimidazolium tetrafluoroborate (EMI-BF_4), and 1-methyl-1-propylpiperidinium bis (trifluoromethylsulfonyl) imide (MPPp-TFSI). The selection of these ionic liquids is largely due to their wider electrochemical stability window and good electric conductivity in comparison with other ionic liquids [20]. Basing on the results obtained in this study, a highest energy density of 169 Wh kg^{-1} was achieved for the graphene electrode in a symmetric supercapacitor charged to 4.4 V using MPPp-TFSI as the electrolyte.

2. Experimental

Graphene oxide (GO) was prepared from graphite using the Hummers method [21]. Single-wall carbon nanotubes were first dispersed by sonication in distilled water using sodium

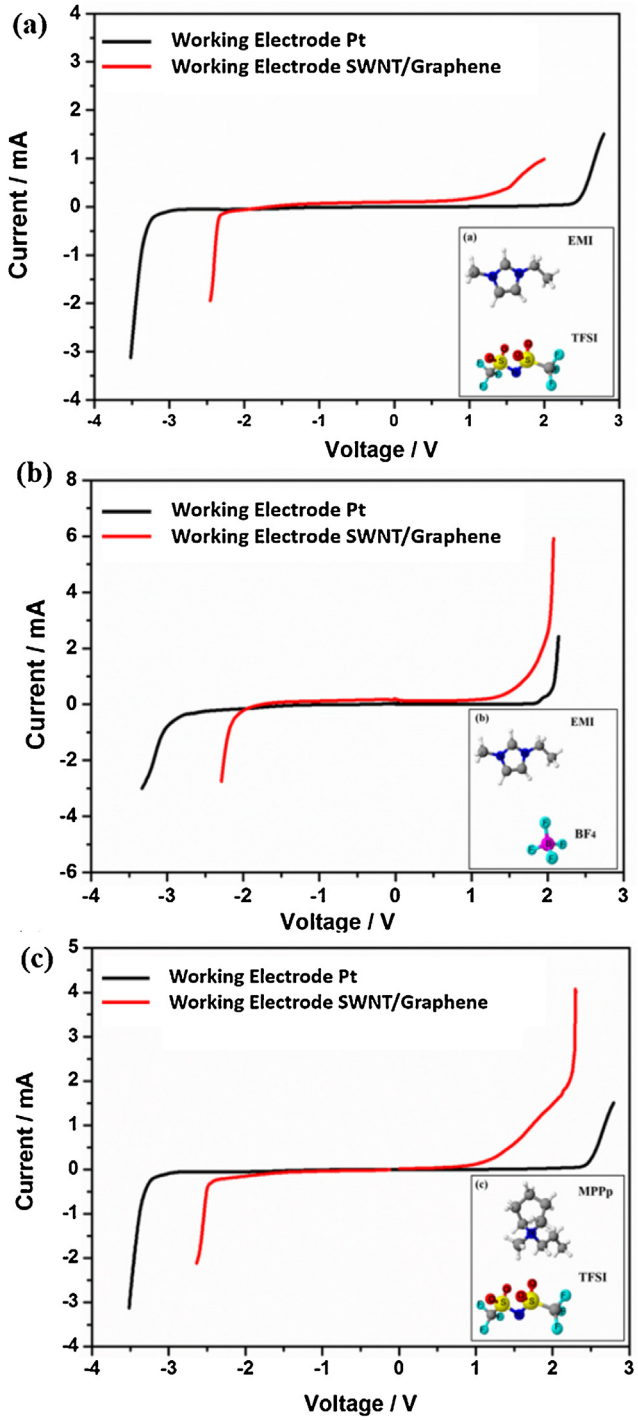

Fig. 1. Electrochemical stability window measured by three-electrode system with working electrode Pt (colored black) and SWNT/graphene (colored red) in (a) EMI-TFSI, (b) EMI-BF_4, and (c) MPPp-TFSI. The inset in each figure shows the chemical structure of respective ionic liquid. (For interpretation of the references to color in this figure legend, the reader is referred to the web version of this article.)

dodecylbenzenesulfonate (SDBS) as surfactant. SWNT/GO composite was then prepared by mixing the dispersions of SWNT and GO powders before it was reduced by hydrazine at 98 °C for 24 hours. The reduced material was rinsed with water and filtered for several times until it became neutral after removing SDBS. The SWNT/graphene composite was eventually obtained as black powders. The coin cell supercapacitor was assembled in the structure as illustrated in Fig. S1 (Supplementary Information).

The ionic liquids with purity 99.9% were purchased commercially (EMI-TFSI from Solvionic, EMI-BF_4 and MPPp-TFSI from Toyo-Gosei). The chemical structure of the ionic liquids was characterized by mass spectroscopy (MS) using AMR Zaplous LC/MS System and Fourier transform infrared spectroscopy (FT-IR) using JASCO FT/IR-6100.

Fig. S1 (Supplementary Information) shows schematically the preparation of electrolyte samples for MS and FT-IR characterization. After completing the charging-discharging process, the electrolyte sample was extracted from the disassembled coin cell supercapacitor using a syringe. For FT-IR characterization, the extracted electrolyte was used directly. For MS characterization, the extracted electrolyte was diluted with acetone to a concentration of 0.2 mol L^{-1}.

The electrode samples were taken directly from the dissembled the coin cell supercapacitor and they were rinsed in acetone and dried in vacuum. The functional groups on the electrode surface were characterized using x-ray photoelectron spectroscopy (XPS; ULVAC-PHI Quantera SXM) with a twin anode Al Kα x-ray source and hemispherical energy analyzer. The energies were calibrated against the aliphatic carbon C1s peak at 284.5 eV.

Electrochemical characterization was carried out using a multi-channel VMP-300 electrochemical workstation.

In order to find out the threshold voltage beyond which electrochemical reactions take place between the ionic liquid electrolyte and the SWNT/graphene electrode during charging, the electrochemical stability window was measured using a three-electrode system with Pt as the counter electrode, silver-silver ion (Ag/Ag^+) as the reference electrode, and Pt or SWNT/graphene composite as the working electrode, respectively. To avoid the interference of water and oxygen in the air, the measurement was carried out in a glove box.

3. Results and Discussion

3.1. Reactions in Electrolyte

Fig. 1 shows the plot of current (mA) vs. voltage (V) acquired experimentally for the three different ionic liquid electrolytes and the results are also summarized in Table 1. The electrochemical stability window herein refers to the range of applied potentials in which no electrochemical reactions would take place. When the working electrode is Pt, the inflection points on the I–V curves (colored black) are due to the decomposition of the ionic liquid electrolyte and therefore the corresponding voltage is the decomposition voltage for each of the three ion liquids: (a) EMI-TFSI (4.6 V), (b) EMI-BF_4 (4.6 V), and (c) MPPp-TFSI (5.8 V) [22]. However, in the same ionic liquid, the inflection point (colored red) started to appear before the electrode reached the decomposition voltage when the SWNT/graphene composite was used as the working electrode as shown in the I–V curves (colored red) in Fig. 1. The inflection points on the red curves are therefore attributed to the electrochemical reactions between the ionic liquid electrolyte and the SWNT/graphene electrode [23].

Table 1
Electrochemical stability window of ionic liquid electrolyte for Pt and SWNT/graphene working electrode.

Electrolytes	Working Electrode	Electrochemical Window
EMI-TFSI	Pt	−2.5 V ~ 2.1 V (Δ=4.6 V)
EMI-TFSI	SWNT/Graphene	−2.4 V ~ 1.3 V (Δ=3.7 V)
EMI-BF_4	Pt	−2.8 V ~ 1.8 V (Δ=4.6 V)
EMI-BF_4	SWNT/Graphene	−2.3 V ~ 1.4 V (Δ=3.7 V)
MPPp-TFSI	Pt	−3.4 V ~ 2.4 V (Δ=5.8 V)
MPPp-TFSI	SWNT/Graphene	−2.4 V ~ 1.6 V (Δ=4.0 V)

As indicated in Fig. 1 and Table 1, electrochemical reactions between the SWNT/graphene electrode and the EMI-TFSI or EMI-BF_4 ionic liquid would occur when the voltage between the two electrodes was in the range of 3.7 and 4.6 V. Electrochemical reactions would occur between the SWNT/graphene electrode and the MPPp-TFSI electrolyte when the voltage between the two electrodes was in the range of 4.0 and 5.8 V using ionic liquid electrolyte MPPp-TFSI.

To study the electrochemical reactions occurred to the EMI-TFSI ionic liquid electrolyte in the charged supercapacitor, we examined the electrolyte that was extracted from the coin cell supercapacitor after it was charged to 4.0 V. Fig. 2 shows the mass spectrum of the extracted electrolyte together with the mass spectrum of pristine ionic liquid EMI-TFSI. As expected, there are only two peaks in the mass spectrum (Fig. 2(a)) of pristine EMI-TFSI with mass-to-charge ratio (m/z) of 111 and 280, corresponding to the EMI^+ and $TFSI^-$ ions, respectively [24]. However, there appeared two additional peaks in the spectrum of used electrolyte (Fig. 2(b)), indicating new products from the electrochemical reactions in used EMI-TFSI. According to the changed mass of the ion from 111 to 129, the new peak at 129 is attributed to an addition to EMI^+ of a hydroxyl group (-OH + H) broken away from the graphene electrode [25] and the new peak at 264 is attributed to the $TFSI^-$ ion losing an oxygen atom, as illustrated in Fig. 3.

To elucidate the chemical nature of the associated changes in the mass of the ions, we employed Fourier transform infrared spectroscopy (FT-IR) to characterize the functional groups. The alkyl C-H stretching peak (2980 cm^{-1}) was normalized as the reference for comparison [26]. In the spectrum of EMI-TFSI (Fig. 4), it can be seen that the peak height corresponding to the double bond between sulfur and oxygen (S=O) decreased after charging. Since $TFSI^-$ is the only source of S=O bond, it indicates that $TFSI^-$ lost oxygen atoms due to breakage of the S=O bond, which is in agreement with the MS analysis. Moreover, the spectrum also showed that a new peak corresponding to the single bond between O and H (O-H) appeared after charging, indicating that certain hydroxyl groups were added to EMI-TFSI. It also agrees well with the MS analysis described above.

Characterization and analysis were also carried out on the pristine EMI-BF_4 and the used EMI-BF_4 electrolyte extracted from a coin cell supercapacitor after charging to 4.2 V. The MS data of EMI-BF_4 before and after charging are shown in Fig. 5. The cation, EMI^+, tends to form a dimer in EMI-BF_4, which results in the peak at 308 in the spectrum of pristine EMI-BF_4 [16,24]. Similarly, since the cation in EMI-BF_4 is the same as that in EMI-TFSI, the peak at 129 also showed up after charging, indicating that a hydroxyl group had been acquired by EMI^+. However, no additional peak related to reaction with BF_4^- was observed. It is therefore suggested that there were no electrochemical reaction between BF_4^- and the SWNT/graphene electrode under charging. It is a significant difference from $TFSI^-$.

More details are reflected in the FT-IR spectrum of EMI-BF_4 (Fig. 6). Compared with EMI-TFSI, when the anion of the ionic liquid was changed to BF_4^-, the peak corresponding to the single bond between O and H (O-H) still showed up in the extracted electrolyte after charging. It supports the assumption that the hydroxyl groups are connected to EMI^+, rather than BF_4^- or TFSI.

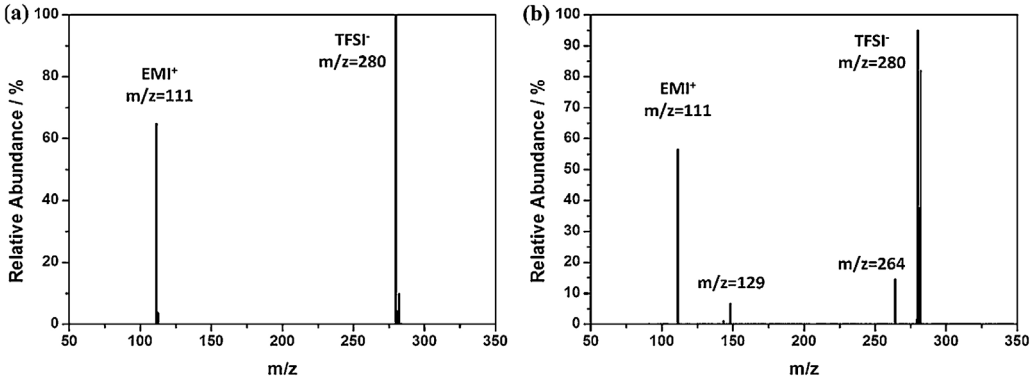

Fig. 2. MS data of EMI-TFSI (a) before and (b) after charging. The new peaks at 129 and 264 in the spectrum (b) after charging indicate additional products from the electrochemical reactions between EMI-TFSI and the SWNT/graphene electrode.

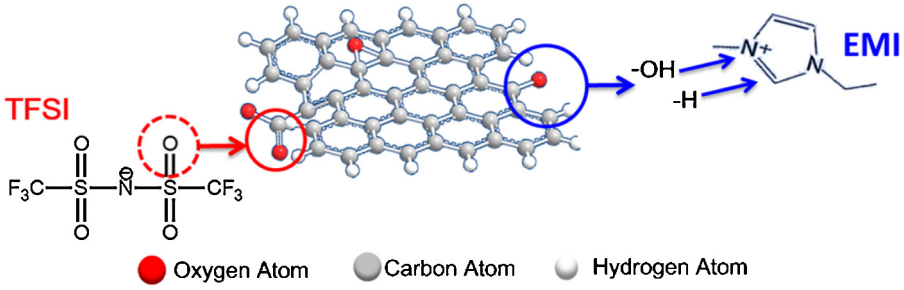

Fig. 3. Schematic of reactions between EMI-TFSI and graphene. Hydroxyl groups from graphene are added to EMI^+ while $TFSI^-$ loses oxygen atoms to graphene.

When using MPPp-TFSI as the electrolyte and comparing with EMI-TFSI, the cation was changed to $MPPp^+$ and the peak at 280 in the MS spectrum (Fig. 7) did not disappear after charging. It therefore indicates that the additional product corresponding to the peak is from electrochemical reactions with $TFSI^-$, rather than EMI^+ or $MPPp^+$. In addition, there was no additional peak arisen from electrochemical reactions related to $MPPp^+$.

Fig. 8 shows the FT-IR data of MPPp-TFSI before and after charging, which agrees with the MS analysis. There was no peak arisen in the range of 3000 and 4000 cm^{-1} after charging, indicating that the hydroxyl groups on the electrode had little reaction with $MPPp^+$ or $TFSI^-$.

The hydroxyl radicals (·OH) and hydrions are assumed to form at the edges of graphene and carbon nanotubes at high voltage and then ·OH would attack the electropositive imidazole ring to have it attached to EMI^+ [25,27,28]. For the loss of sulfonyl oxygen in $TFSI^-$, the S=O bond might be protonated to S-OH first and then –OH would attack the attached heteroatoms in graphene and carbon nanotubes while breaking-up the S-O bond at the same time [28–32].

3.2. Reactions on Electrode

Besides the electrolyte, electrochemical reactions also occurred on the SWNT/graphene electrode, which would in turn affect the performance of the graphene supercapacitor. FT-IR and XPS were applied to analyze the electrochemical reactions occurred on the SWNT/graphene electrode, which was taken out from the coin cell supercapacitor after charging. Results of analysis were compared

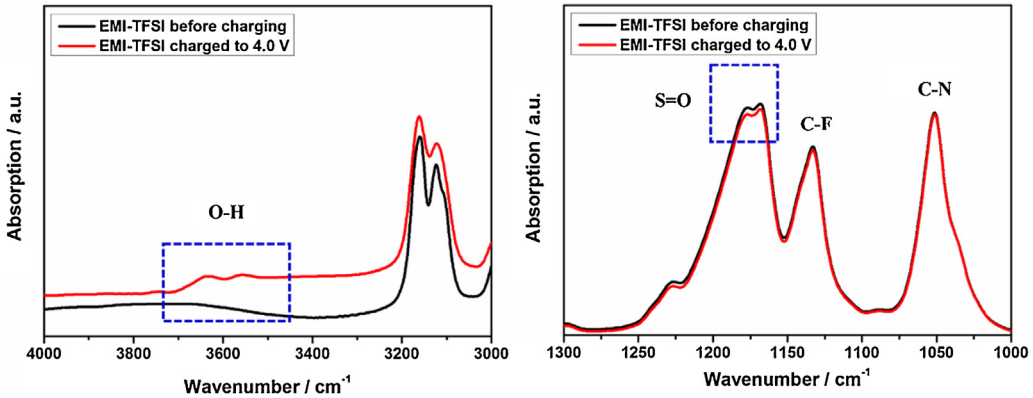

Fig. 4. FT-IR data of EMI-TFSI before and after charging. The peak in the range of 3500 and 3700 cm^{-1} indicates existence of hydroxyl groups in EMI-TFSI after charging. The decrease of the S=O peak after charging indicates that $TFSI^-$ loses oxygen atoms as S=O bond breakage occurrs.

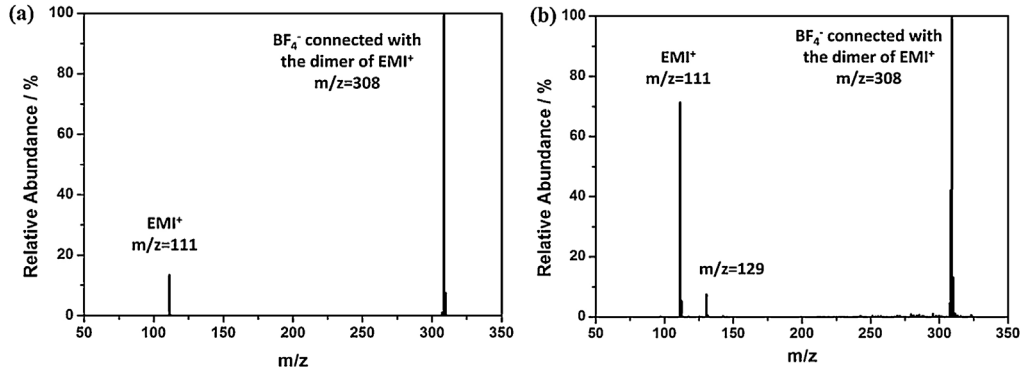

Fig. 5. MS data of EMI-BF_4 (a) before and (b) after charging. The peak at 129 is due to reaction with EMI^+ after acquiring a hydroxyl group.

before and after charging of the SWNT/graphene electrode in order to find out the differences of the functional groups on the SWNT/graphene electrode using different ionic liquid electrolyte.

Fig. 9 shows the FT-IR data taken from the graphene electrode before and after charging from 0 to 4.0 V in EMI-TFSI electrolyte. In the spectrum the intensity of the peak corresponding to the bond between the carbon atoms (C=C) in the hexatomic ring is normalized as the reference for comparison. It can be seen that the peaks corresponding to the single bond between carbon and oxygen (C-O) and the single bond between oxygen and hydrogen (O-H) on the electrode decreased more than 50%, while the peak corresponding to the double bond between carbon and oxygen (C=O) increased after charging in the EMI-TFSI electrolyte. Combining with the FT-IR analysis of EMI-TFSI, we suggest that the reduced peaks are due to the breakage of bonds between the hydroxyl groups and carbon atoms on the SWNT/graphene electrode and that the detached hydroxyl groups were added to EMI-TFSI. At the same time, the lost oxygen atoms from $TFSI^-$ became associated with the carbon atoms in SWNT/graphene by double bond, which resulted in an increase of the corresponding peak in the FT-IR spectrum.

As for the ionic electrolyte EMI-BF_4, as shown in Fig. 10, the peak corresponding to the single bond between oxygen and hydrogen (O-H) decreased after charging, which is similar to the results in EMI-TFSI. It is attributed to a reaction in which the hydroxyl group from graphene is captured by EMI^+ under charging. At the same time, the peak due to the double bond between carbon and oxygen (C=O) in graphene stayed unchanged after charging, different from the graphene electrode charged in EMI-TFSI. Combining with the MS results, it showed that EMI-BF_4 had little reaction with the functional groups on graphene.

Different from graphene electrode charged in EMI-TFSI and EMI-BF_4, the FT-IR (Fig. 11) results showed that the peak corresponding to the single bond between oxygen and hydrogen (O-H) remained the same after charging in the MPPp-TFSI electrolyte. It therefore indicates that the reduction of hydroxyl groups on the SWNT/graphene electrode is due to reactions with EMI^+ rather than $MPPp^+$.

Fig. S2 (Supplementary Information) shows the C1s spectra of the parent SWNT/graphene electrode and the activated electrode after electrochemical loading. The decreased ratio of C-OH peak at 285.6 eV in electrode charged in EMI-TFSI and EMI-BF_4 supplements the FT-IR results [9]. Besides, the O/C ratio increased from 22.8% to 27.7% after charging in MPPp-TFSI. Combining with the characterization results of the electrolyte, the increased oxygen on the SWNT/graphene electrode is attributed to the breakage of the S=O bond in $TFSI^-$.

Given the close similarity in bonding between the carbon atoms, it should be noted that the electrochemical reactions discussed above could take place in both graphene and SWNTs interchangeably.

3.3. Influence on Performance of Supercapacitor

In the cyclic voltammetry (CV) measurement, a chemical reaction would result in a sudden change in the electric current, which is reflected as a redox peak on the CV curve. From the CV diagram, we can therefore expect that, when the voltage applied on the supercapacitor is larger than 3.7 V, redox peaks could appear on the CV curves for EMI-TFSI and EMI-BF_4 electrolyte due to the occurrence of chemical reactions.

However, redox peaks also appeared on the CV curves with MPPp-TFSI electrolyte even when the applied voltage was smaller than the threshold voltage required for chemical reactions with MPPp-TFSI (4.0 V). These redox peaks are attributed to the physical interactions between the electrolyte ions and the structural pores in the active material of the electrode [33–35]. Considering the fact that the size of $MPPp^+$ is larger than EMI^+, chemical reactions may be not the only interaction between MPPp-TFSI and graphene [35]. Physical interactions between pores and ions in MPPp-TFSI electrolyte are also possible to take a dominant role in the two kinds of interactions, resulting in the peaks on the CV curves of MPPp-TFSI subjected to a lower voltage. For example, penetration of ions into the pores smaller than the ions is possible [36,37].

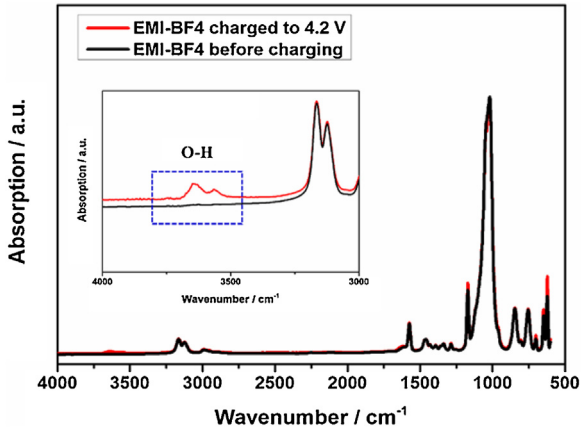

Fig. 6. FT-IR of EMI-BF_4 before and after charging. More hydroxyl groups are observed after charging.

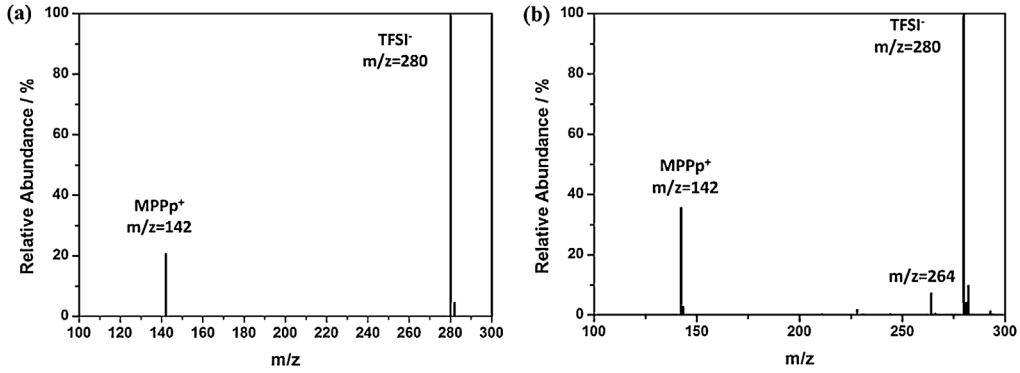

Fig. 7. MS data of MPPp-TFSI (a) before and (b) after charging. The peak at 264 is due to reaction with $TFSI^-$ after it loses an oxygen atom.

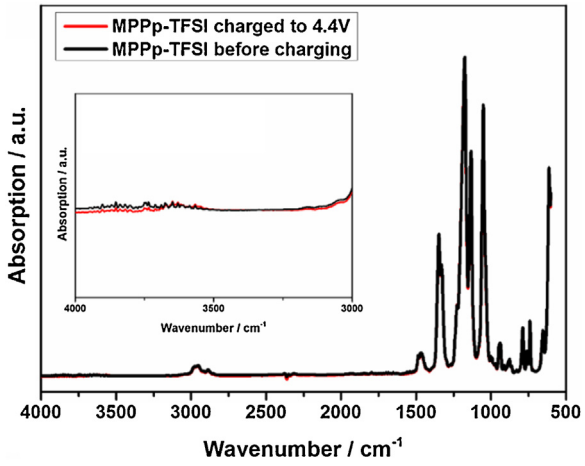

Fig. 8. FT-IR data of MPPp-TFSI before and after charging. No significant change due to charging is observed.

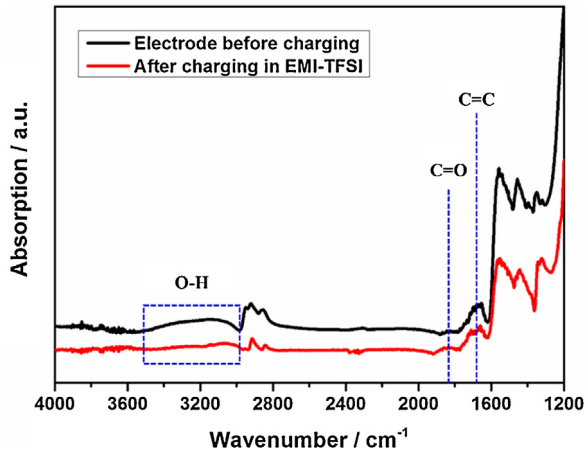

Fig. 9. FT-IR data of SWNT/graphene electrode before and after charging in EMI-TFSI. The peak corresponding to the hydroxyl group has an obvious drop, indicating that some of the hydroxyl groups were removed from the graphene electrode after charging.

Table 2 lists the specific capacitance and energy density of the graphene supercapacitor calculated from the charge-discharge curves (Fig. 12) at the current density of 0.2 A g^{-1}. The supercapacitor with EMI-TFSI electrolyte has a larger specific capacitance under the same charged voltage. Considering that there are more reactions between EMI-TFSI and graphene, it implies that the chemical species due to both the ionic liquid and the graphene electrode contributed to the larger capacitance. On the other hand, the largest energy density was achieved in the supercapacitor using the MPPp-TFSI electrolyte when the applied voltage reached 4.4 V. Even though the specific capacitance with MPPp-TFSI electrolyte is smaller than that with EMI-TFSI and EMI-BF_4 electrolyte, the electrochemical stability window and therefore the operating voltage is larger with the MPPp-TFSI electrolyte to lead to the highest energy density of 169 Wh kg^{-1}.

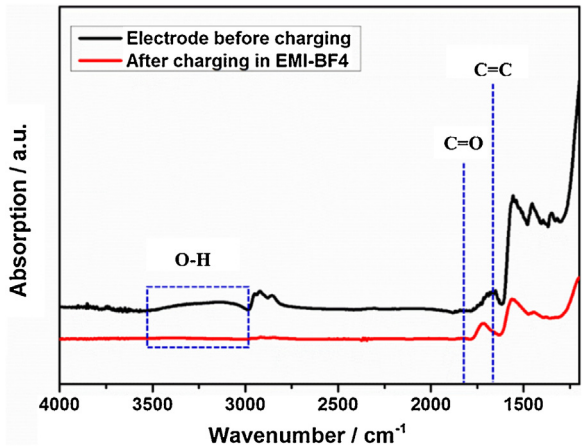

Fig. 10. FT-IR data of SWNT/graphene electrode before and after charging in EMI-BF_4 electrolyte.

4. Conclusions

Measurement of electrochemical stability windows revealed that electrochemical reactions took place between the ionic liquid electrolyte and the SWNT/graphene electrode when the applied voltage was in the range of 3.7 and 4.6 V for EMI-TFSI and EMI-BF_4. For MPPp-TFSI electrolyte, electrochemical reactions occurred in the range of 4.0 and 5.8 V. Using mass spectroscopy and Fourier transform infrared spectroscopy, we determined that the hydroxyl groups from SWNT/graphene were transferred to EMI^+ and $TFSI^-$ would lose oxygen atoms to SWNT/graphene during charging, while little reaction occurred to BF_4^- and $MPPp^+$.

The electrochemical reactions will affect the performance of graphene supercapacitors and they are one of the reasons for the

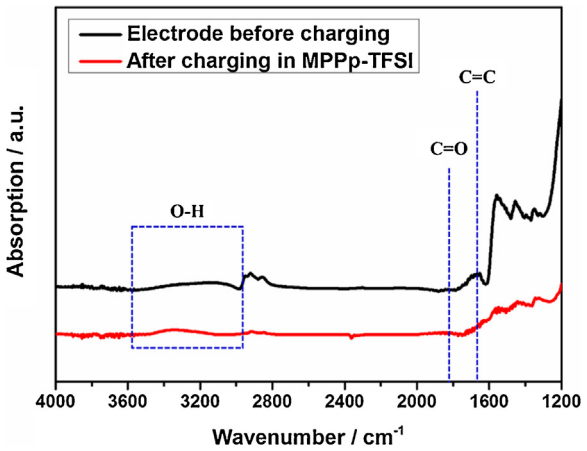

Fig. 11. FT-IR data of SWNT/graphene electrode before and after charging in MPPp-TFSI electrolyte.

Table 2
Performance of graphene supercapacitors with different ionic liquid electrolyte.

Voltage (V)	Ionic Liquids	Specific Capacitance (F/g)	Energy Density (Wh/kg)
3.7	EMI-TFSI	243	112
	EMI-BF4	174	81
	MPPp-TFSI	151	69
4.0	EMI-TFSI	332	156
	EMI-BF4	197	105
	MPPp-TFSI	146	78
4.2	EMI-BF4	260	145
	MPPp-TFSI	217	129
4.4	MPPp-TFSI	258	169

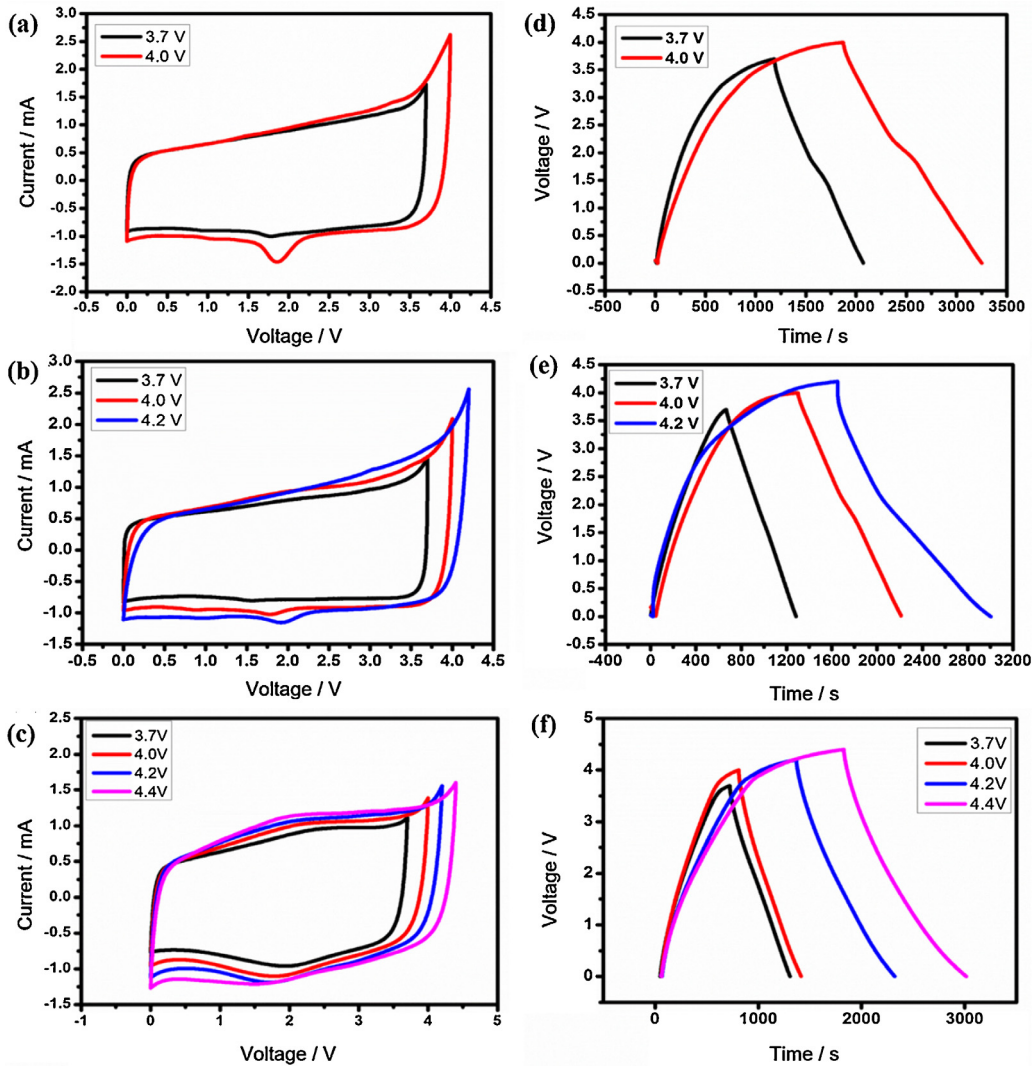

Fig. 12. CV of supercapacitor with (a) EMI-TFSI, (b), EMI-BF_4, and (c) MPPp-TFSI electrolyte. The corresponding charge-discharge curves measured at current density of 0.2 A g^{-1} are given in (d-f).

decreased electrochemical stability window. The largest specific capacitance under the same voltage was achieved in EMI-TFSI electrolyte while the highest energy density of 169 Wh kg^{-1} was achieved in MPPp-TFSI electrolyte due to a higher operating voltage of 4.4 V.

Acknowledgements

This work was financially supported by the JST ALCA Program (No. 22310074), JSPS Grants-in-Aid for Scientific Research (No. 22310074), the Nanotechnology Network Project of MEXT, Japan, and Provincial Natural Science Foundation (No. LY14E020010) of Zhejiang, China.

Appendix A. Supplementary data

Supplementary data associated with this article can be found, in the online version, at http://dx.doi.org/10.1016/j.electacta.2016.03.036.

References

[1] G.P. Wang, L. Zhang, J.J. Zhang, Chem. Soc. Rev. 41 (2012) 797–828.
[2] L.L. Zhang, X.S. Zhao, Chem. Soc. Rev. 38 (2009) 2520–2531.
[3] M. Liang, F.M. Jin, R. Liu, R.X. Su, W. Qi, Y.J. Yu, L.B. Wang, Z.M. He, J. Mater. Sci. 48 (2013) 5624–5632.
[4] H. Pan, J.Y. Li, Y.P. Feng, Nanoscale Res. Lett. 5 (2010) 654–668.
[5] L.M. Dai, D.W. Chang, J.-B. Baek, W. Lu, Small 8 (2012) 1130–1166.
[6] C.G. Liu, Z.N. Yu, D. Neff, A. Zhamu, B.Z. Jang, Nano Lett. 10 (2010) 4863–4868.
[7] Q. Cheng, J. Tang, J. Ma, H. Zhang, N. Shinya, L.-C. Qin, Phys. Chem. Chem. Phys. 13 (2011) 17615–17624.
[8] J.B. Hou, Y.Y. Shao, M.W. Ellis, R.B. Moored, B.L. Yi, Phys. Chem. Chem. Phys. 13 (2011) 15384–15402.
[9] D.R. Dreyer, S. Park, C.W. Bielawski, R.S. Ruoff, Chem. Soc. Rev. 39 (2010) 228–240.
[10] J. Yan, T. Wei, B. Shao, F.Q. Ma, Z.J. Fan, M.L. Zhang, C. Zheng, Y.C. Shang, W.Z. Qian, F. Wei, Carbon 48 (2010) 1731–1737.
[11] F.F. Zhang, J. Tang, N. Shinya, L.-C. Qin, Chem. Phys. Lett. 584 (2013) 124–129.
[12] M. Armand, F. Endres, D. R. MacFarlane, H. Ohno, and B. Scrosati, Nature Mater. 8 (2009) 621–629. K. P. Gong, S. Chakrabarti, and L. M. Dai, Angew. Chem. Int. Ed. 47 (2008) 5446–5450.
[13] R. Kotz, M. Carlen, Electrochim. Acta 45 (2000) 2483–2498.
[14] M. Vijayakumar, B. Schwenzer, V. Shutthanandan, J.Z. Hu, J. Liu, I.A. Aksay, Nano Energy 3 (2014) 152–158.
[15] S. Kerisit, B. Schwenzer, M. Vijayakumar, J. Phys. Chem. Lett. 5 (2014) 2330–2334.
[16] T. Romann, O. Oll, P. Pikma, H. Tamme, E. Lust, Electrochim. Acta 125 (2014) 183–190.
[17] W. Ai, X.H. Cao, Z.P. Sun, J. Jiang, Z.Z. Du, L.H. Xie, Y.L. Wang, X.J. Wang, H. Zhang, W. Huang, T. Yu, J. Mater. Chem. A 2 (2014) 12924–12930.
[18] Y.S. Ye, H. Wang, S.G. Bi, Y. Xue, Z.G. Xue, Y.G. Liao, X.P. Zhou, X.L. Xie, Y.W. Mai, Carbon 86 (2015) 86–97.
[19] Q. Shao, J. Tang, Y. Lin, J. Li, F. Qin, K. Zhang, J. Yuan, L.-C. Qin, Electrochim. Acta 176 (2015) 1441–1446.
[20] S. Zhang, N. Sun, X. He, X. Lu, X. Zhang, J. Phys. Chem. Ref. Data 35 (2006) 1475–1517.
[21] W.S. Hummers, R.E. Offeman, J. Am. Chem. Soc. 80 (1958) 1339.
[22] G.B. Appetecchi, M. Montaninoa, D. Zaneb, M. Carewska, F. Alessandrini, S. Passerini, Electrochim. Acta 54 (2009) 1325–1332.
[23] X.Z. Yuan, V. Alzate, Z. Xie, D.G. Ivey, E. Dy, W. Qua, J. Electrochem. Soc. 161 (2014) 458–466.
[24] C.Y. Kong, W.Z. Qian, C. Zheng, Y.T. Yu, C.J. Cui, F. Wei, Chem. Commun. 49 (2013) 10727–10729.
[25] J. Llano, L.A. Eriksson, J. Phys. Chem. B 103 (1999) 5598–5607.
[26] X. Chen, J. Zhao, J. Zhang, L. Qiu, D. Xu, H. Zhang, X. Han, B. Sun, G. Fu, Y. Zhang, F. Yan, J. Mater. Chem. 22 (2012) 18018–18024.
[27] T. Kuila, A.K. Mishra, P. Khanra, N.H. Kim, J.H. Lee, Nanoscale 5 (2013) 52–71.
[28] L. Chen, Y. Tang, K. Wang, C. Liu, S. Luo, Electrochem. Commun. 13 (2011) 133–137.
[29] R.L. Carlson, R.S. Drago, J. Am. Chem. Soc. 84 (1962) 2320–2323.
[30] W. Ying, D.D. DesMarteau, Y. Gotoh, Tetrahedron 52 (1996) 15–22.
[31] P. Kielbasinski, J. Drabowicz, M. Mikolajczyk, J. Org. Chem. 47 (1982) 4806–4808.
[32] J.-C. Lassegues, J. Grondin, C. Aupetit, P. Johansson, J. Phys. Chem. A 113 (2009) 305–314.
[33] H.-C. Huang, C.-W. Huang, C.-T. Hsieh, H. Teng, J. Mater. Chem. A 2 (2014) 14963–14972.
[34] J. Chmiola, C. Largeot, P.-L. Taberna, P. Simon, Y. Gogotsi, Angew. Chem. Int. Ed. 47 (2008) 3392–3395.
[35] A. Bhattacharjee, P.J. Carvalho, J.A.P. Coutinho, Fluid Phase Equilibria 375 (2014) 80–88.
[36] H. Zhang, G. Cao, Y. Yang, Z. Gu, J. Electrochem. Soc. 155 (2008) 19–22.
[37] C.-M. Yang, H.J. Jung, Y.J. Kim, J. Colloid Interface Sci. 446 (2015) 208-2.